iScience

CellPress
OPEN ACCESS

Article

GAS5-inhibited hepatocyte pyroptosis contributes to hepatic stellate cell inactivation via microRNA-684 and AHR

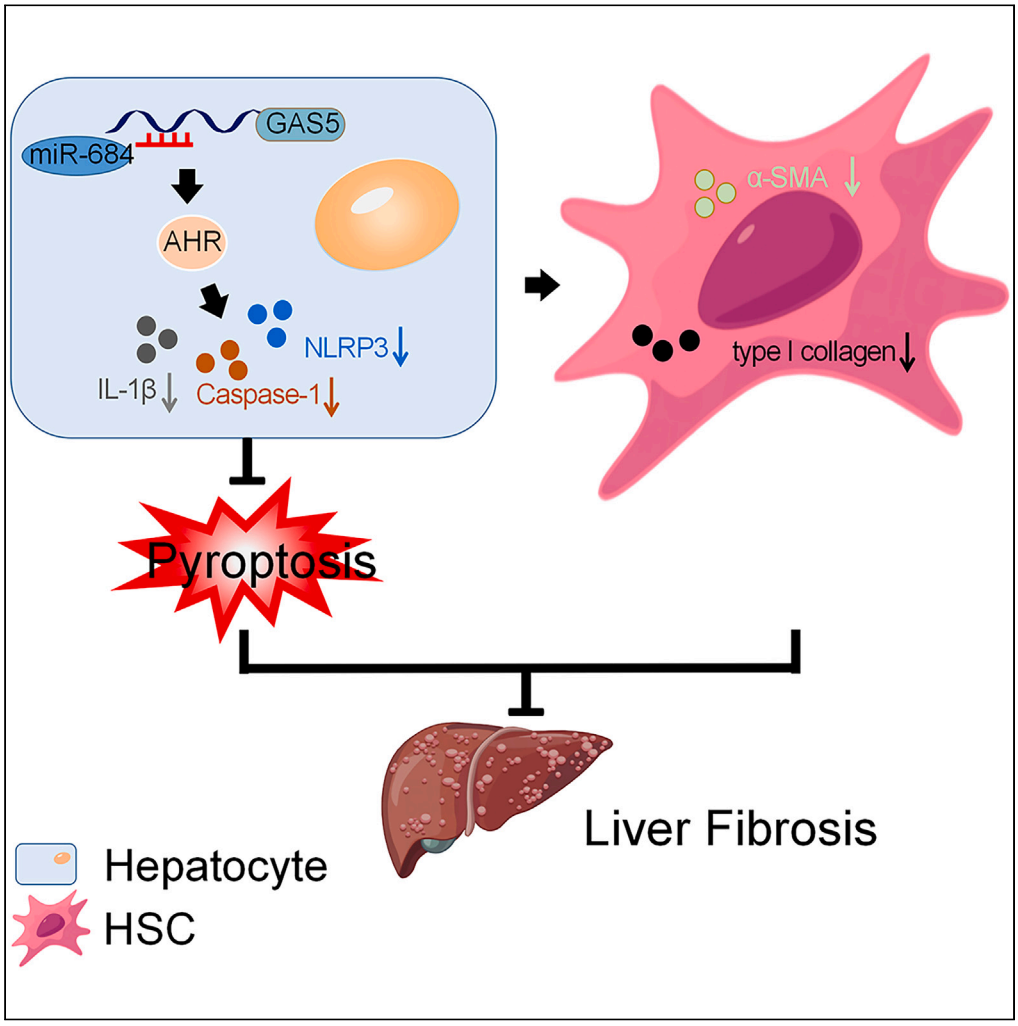

Zhichao Lang, Rongrong Zhang, Xinmiao Li, ..., Lei Zheng, Zhixian Yu, Jianjian Zheng

yuzhixian@wmu.edu.cn (Z.Y.)
zjj@wmu.edu.cn (J.Z.)

Highlights

GAS5-inhibited liver fibrosis is associated with NLRP3-mediated hepatocyte pyroptosis

GAS5 inhibits hepatocyte pyroptosis via regulation of miR-684 and its target AHR

Hepatocyte pyroptosis suppresses HSC activation and liver fibrosis

Lang et al., iScience 26, 107326
August 18, 2023
https://doi.org/10.1016/j.isci.2023.107326

iScience

CellPress
OPEN ACCESS

Article

GAS5-inhibited hepatocyte pyroptosis contributes to hepatic stellate cell inactivation via microRNA-684 and AHR

Zhichao Lang,[1] Rongrong Zhang,[1] Xinmiao Li,[1] Yan Jin,[1] Yuhang Hu,[2] Xinyi Lin,[1] Yunzhi Tang,[1] Jingnan Zhang,[1] Lei Zheng,[1,3] Zhixian Yu,[4,*] and Jianjian Zheng[1,2,5,*]

SUMMARY

Hepatocyte pyroptosis has been shown to be involved in liver damage progression. Previously, we found that growth arrest-specific 5 (GAS5) is a regulator of hepatic stellate cell (HSC) activation. However, whether GAS5 plays a role in hepatocyte pyroptosis remains unclear. In this study, reduced GAS5 was shown in CCl_4-treated mice and restoration of GAS5-inhibited liver fibrosis *in vivo*. Hepatocyte pyroptosis participated in the effects of GAS5-inhibited liver fibrosis, associated with reduced caspase-1, NLRP3, and IL-1β (hepatocyte pyroptosis markers). Notably, AHR expression, a suppressor of NLRP3, was enhanced by GAS5. Silencing AHR inhibited GAS5-mediated hepatocyte pyroptosis. GAS5 and AHR were targets of microRNA-684 (miR-684). In addition, the effects of GAS5 on hepatocyte pyroptosis could be inhibited by miR-684. Interestingly, GAS5-mediated hepatocyte pyroptosis contributed to HSC inactivation. In conclusion, we demonstrate that GAS5 inhibits hepatocyte pyroptosis and HSC activation, at least in part, via regulation of miR-684 and AHR.

INTRODUCTION

Generally, liver damage contributes to liver fibrosis progression, which may develop into liver cirrhosis.[1] Hepatocyte cell death represents a critical event involved in resultant inflammation and disease progression in various acute and chronic liver disorders.[2,3] It has been reported that pyroptosis correlates with the degree of hepatic damage and plays a crucial role in liver diseases.[2] Pyroptosis is a caspase-1-dependent programmed cell death, characterized by cell swelling, rapid rupture of plasma-membrane and diffusion of proinflammatory intracellular contents.[4] A previous study revealed that persistent NLR family pyrin domain-containing 3 (NLRP3) inflammasome activation induces hepatocyte pyroptosis and severe liver damage in NLRP3 knock-in mice.[5] Therefore, it is of great significance to explore the role of hepatocyte pyroptosis in liver fibrosis.

Increasing evidence has demonstrated that NLRP3, which activates the inflammasome, participates in the development of pyroptosis.[6] The inflammasome, a multiprotein oligomer, contributes to the activation of inflammatory responses.[7] It is known that NLRP3 inflammasome is composed of ASC, Nek7, and caspase-1.[8] Caspase-1 has been reported to cleave the gasdermin-N and -C domains of gasdermin-D (GSDMD).[9] Caspase-1 has also been reported to mediate the maturation of interleukin 1 beta (IL-1β) and IL-18, thus allowing the inflammatory process to be finally performed as pyroptosis.[6] Interestingly, IL-1β has been demonstrated to enhance the activation of hepatic stellate cells (HSCs), which predominates the process of liver fibrosis.[10,11] Notably, increasing evidence has shown the correlations between hepatocyte pyroptosis and HSC activation. Gaul et al. demonstrated that hepatocyte pyroptosis contributes to HSC activation and liver fibrosis.[2]

Long non-coding RNA-Growth arrest-specific 5 (lncRNA-GAS5), as a tumor suppressor, is involved in the development of various human cancers such as breast cancer, prostate cancer, and epithelial ovarian cancer.[12–14] GAS5 has been reported to exert anti-cancerous effects in liver cancer via microRNA-382-3p (miR-382-3p) and cytochrome P450 family 2 subfamily C member 8.[15] Han et al. reported that the level of GAS5 is correlated with the progression of liver fibrosis.[16] Previously, we found that GAS5 could act as a regulator of HSC activation.[17] Interestingly, Mo et al. found that GAS5 could promote pyroptosis in chronic obstructive

[1]Key Laboratory of Clinical Laboratory Diagnosis and Translational Research of Zhejiang Province, the First Affiliated Hospital of Wenzhou Medical University, Wenzhou 325000, China

[2]Cixi Biomedical Research Institute, Wenzhou Medical University, Ningbo 315300, China

[3]Laboratory Medicine Center, Nanfang Hospital, Southern Medical University, Guangzhou 510515, China

[4]Department of Urology, the First Affiliated Hospital of Wenzhou Medical University, Wenzhou 325000, China

[5]Lead contact

*Correspondence: yuzhixian@wmu.edu.cn (Z.Y.), zjj@wmu.edu.cn (J.Z.)

https://doi.org/10.1016/j.isci.2023.107326

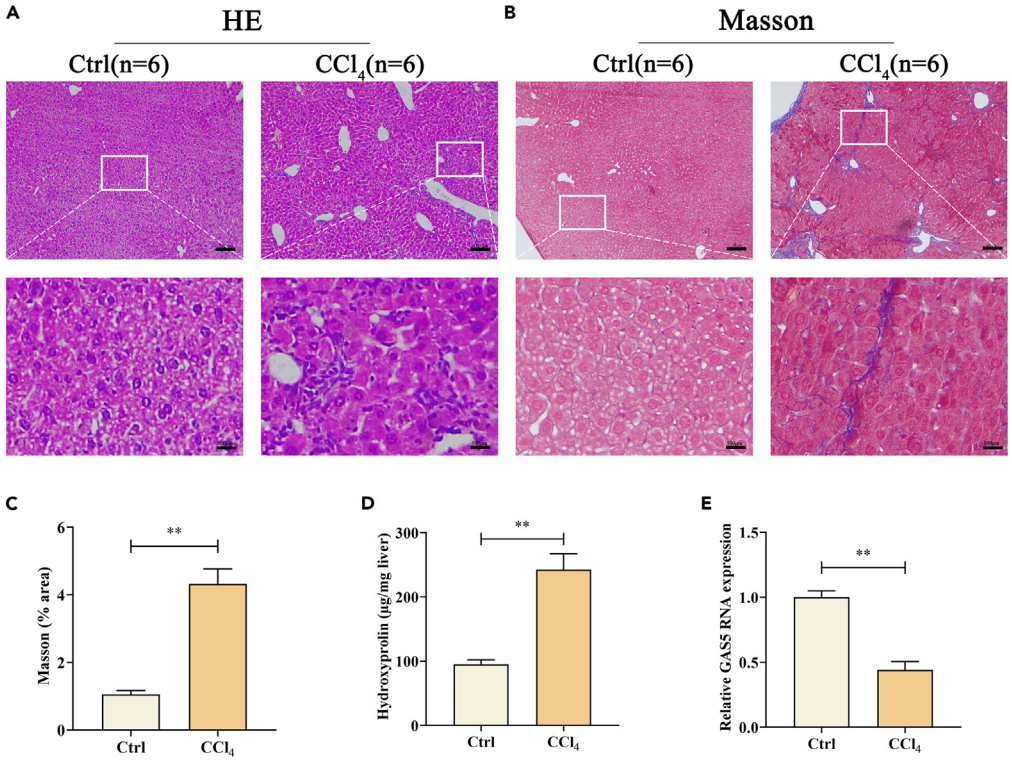

Figure 1. Successful establishment of the CCl_4-induced mouse liver fibrosis model and reduction of GAS5 in the liver tissues of CCl_4-treated mice

(A) HE staining for evaluating liver fibrosis model. Scale bar: 100 μm; Enlarge: 500 μm.

(B and C) Masson staining for assessing collagen deposition. Scale bar: 100 μm; Enlarge: 500 μm.

(D) Hydroxyproline level.

(E) GAS5 expression. Ctrl group (n = 6), CCl_4 group (n = 6). Data are represented as mean ± SD and two-tailed Student's *t* test was used to assess the significance. **p < 0.01, versus Ctrl group.

pulmonary disease.[18] It is interesting whether hepatocyte pyroptosis is involved in the effects of GAS5-inhibited liver fibrosis.

RESULTS

Successful establishment of the CCl_4-induced mouse liver fibrosis model and reduction of GAS5 in the liver tissues of CCl_4-treated mice

To determine the level of GAS5 during liver fibrosis, CCl_4, commonly used for fibrosis induction, was used to induce liver fibrosis in mice.[19] As shown in Figure 1A, the results of hematoxylin and eosin (HE) indicated infiltration of inflammatory cells and abnormal liver cell arrangement in CCl_4-treated mice in comparison with the control group. Analysis of Masson staining revealed the increased blue area in CCl_4-induced mice, suggesting the accumulation of collagen caused by CCl_4 (Figures 1B and 1C). CCl_4-induced collagen was further confirmed by hydroxyproline assays (Figure 1D). In addition, higher activation was found in HSCs isolated from CCl_4-induced mice (Figure S1A). All the results confirmed the establishment of the CCl_4-induced mouse liver fibrosis model. Next, the expression of GAS5 was examined in the fibrotic livers. It was found that GAS5 was reduced in the liver tissues of CCl_4-treated mice (Figure 1E). Clearly, there was a significant reduction in GAS5 level in CCl_4-induced liver fibrosis, indicating the involvement of GAS5 in liver fibrosis progression.

GAS5-inhibited liver fibrosis is associated with NLRP3-mediated hepatocyte pyroptosis *in vivo*

Given that GAS5 may participate in the development of liver fibrosis, the effects of over-expressing GAS5 on liver fibrosis caused by CCl_4 were examined. Adenoviral vectors expressing GAS5 (Ad-GAS5) was

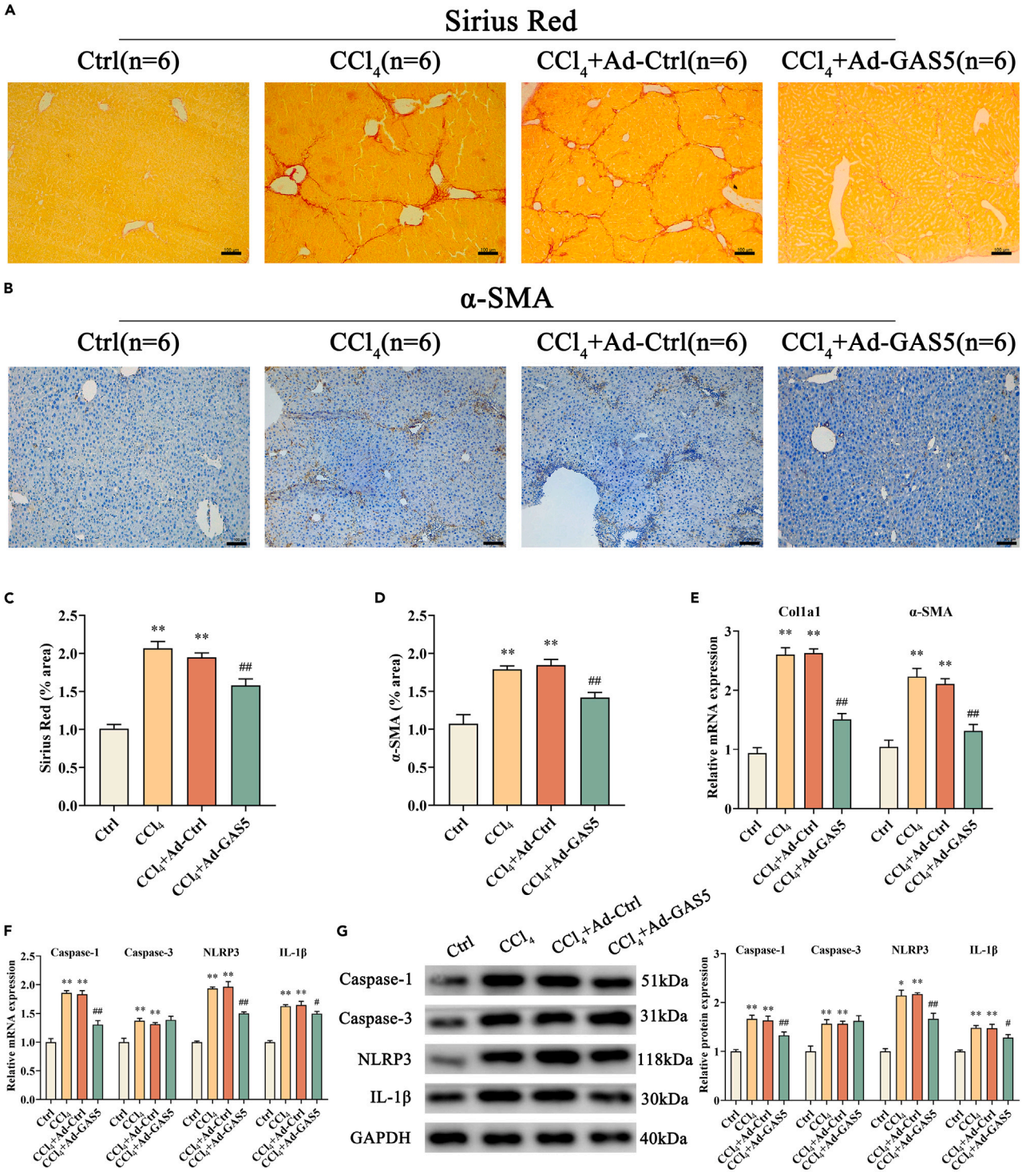

Figure 2. GAS5-inhibited liver fibrosis is associated with NLRP3-mediated hepatocyte pyroptosis *in vivo*

(A and C) Analysis of Sirius Red staining for collagen deposits. Scale bar: 100 μm.

(B and D) Analysis of α-SMA immunohistochemistry. Scale bar: 100 μm.

(E) mRNA expression levels of Col1A1 and α-SMA in liver tissues.

(F) mRNA expression levels of Caspase-1, Caspase-3, NLRP3, and IL-1β in primary hepatocytes.

Figure 2. *Continued*

(G) Protein levels of Caspase-1, Caspase-3, NLRP3, and IL-1β in primary hepatocytes. Ctrl group (n = 6), CCl_4 group (n = 6), CCl_4+adenoviral vectors expressing a control scrambled sequence (Ad-Ctrl) group (n = 6), CCl_4+Ad-GAS5 group (n = 6). Data are represented as mean ± SD and one-way ANOVA was used to assess the significance. *p < 0.05, **p < 0.01, versus Ctrl group; $^{\#}p < 0.05$, $^{\#\#}p < 0.01$, versus CCl_4+Ad-Ctrl group.

delivered into CCl_4-treated mice and expression of GAS5 was shown to be significantly increased by Ad-GAS5 (Figure S1B). Notably, results of Sirius Red staining demonstrated that GAS5 overexpression inhibited CCl_4-mediated collagen accumulation (Figures 2A and 2C). As indicated by Figures 2B and 2D, α-smooth muscle actin (α-SMA) immunohistochemical analysis showed that GAS5 inhibited α-SMA induced by CCl_4. In line with it, the results of quantitative real-time PCR (qRT-PCR) showed that α-SMA mRNA as well as collagen type I alpha 1 chain (Col1A1) mRNA in CCl_4-treated mice was suppressed by GAS5 overexpression (Figure 2E). In addition, GAS5 treatment improved liver injury, with a reduction in alanine aminotransferase (ALT) and aspartate aminotransferase (AST) (Figures S1C and S1D). Combined with these, our data suggest that GAS5 could inhibit CCl_4-induced liver fibrosis and liver injury.

Accumulating studies have demonstrated that hepatocyte pyroptosis is involved in the progression of liver fibrosis.[20,21] Whether GAS5-inhibited liver fibrosis is associated with hepatocyte pyroptosis was next examined. The expressions of markers of pyroptosis (caspase-1, NLRP3, and IL-1β) as well as apoptosis marker (caspase-3) were analyzed in primary hepatocytes isolated from CCl_4-treated mice after GAS5 overexpression treatment. We found that the mRNA and protein expression levels of caspase-1, caspase-3, NLRP3, and IL-1β were enhanced in primary hepatocytes isolated from CCl_4-treated mice (Figures 2F and 2G). In hepatocytes, CCl_4-induced markers of pyroptosis were inhibited by GAS5, whereas CCl_4-mediated apoptosis markers not. Similar results were also observed in immunofluorescence analysis, with reduced markers of pyroptosis, including in CCl_4+Ad-GAS5 group (Figure S2). Taken together, we demonstrate the involvement of NLRP3-mediated pyroptosis in the effects of GAS5 on the suppression of CCl_4-induced liver fibrosis.

Aryl hydrocarbon receptor (AHR) is involved in the effects of GAS5-inhibited hepatocyte pyroptosis

It is well known that NLRP3 plays a key role in the initiation of pyroptosis.[22,23] It is interesting whether the suppressors of NLRP3 (AHR, SIRT2, and MUL1) take part in the effects of GAS5-inhibited hepatocyte pyroptosis. It was found that Ad-GAS5 treatment induced a significant increase in GAS5 level in primary hepatocytes (Figure S3A). Overexpression of GAS5 led to an increase in the mRNA level of AHR, with no change in SIRT2 and MUL1 (Figure 3A). Similarly, enhanced AHR protein was found in the Ad-GAS5 group (Figure 3B). Subsequently, the effects of loss of GAS5 on hepatocyte pyroptosis and AHR were examined. As indicated by Figure S3B, the level of GAS5 in primary hepatocytes was significantly reduced after adenovirus vectors expressing shRNA anti-GAS5 (Ad-shGAS5) treatment. It was found that the mRNA and protein expression levels of caspase-1, NLRP3, and IL-1β were up-regulated by silencing of GAS5, respectively (Figures 3C and 3D). Our results further confirmed the involvement of GAS5-mediated pyroptosis in hepatocytes. Importantly, reduced AHR was also shown in the Ad-shGAS5 group (Figures 3C and 3D), suggesting the key role of AHR in GAS5-mediated hepatocyte pyroptosis. Collectively, GAS5 inhibits hepatocyte pyroptosis, at least in part, via AHR.

GAS5 is a target of miR-684

LncRNAs have been demonstrated to sponge miRNAs and then derepress the targets of miRNAs via the mechanisms of competing for endogenous RNAs (ceRNAs).[24] As shown in Figure 4A, higher GAS5 was found in the cytoplasm of hepatocytes in comparison with that in the nucleus. Whether GAS5 serves as a ceRNA to mediate the activity of miRNAs was examined. Obviously, analysis of the RNA-binding protein immunoprecipitation (RIP) indicated that GAS5 was enriched in the Ago2 pellet compared with that in immunoglobulin G (IgG) pellets (Figure 4B). Clearly, GAS5 could serve as a binding platform for Ago2 as well as miRNAs. Bioinformatic analysis (Miranda and RNAhybrid), which could predict the potential GAS5-binding miRNAs, showed that miRNAs including miR-32-3p, miR-124-3p, miR-205-5p, miR-323-3p, miR-375-3p, miR-425-3p, miR-684, and miR-759, were predicted to bind GAS5. As indicated by Figure 4C, miR-205-5p, miR-375-3p, and miR-684 were found to be reduced by GAS5, with the lowest expression in miR-684. Further studies were performed to determine the relationship between miR-684 and GAS5. Luciferase activity assays showed that the luciferase reporter activities of GAS5 wild type (GAS5-Wt) were inhibited by miR-684 (Figure 4D). In addition, miR-205-5p and miR-375-3p did not affect GAS5-Wt luciferase

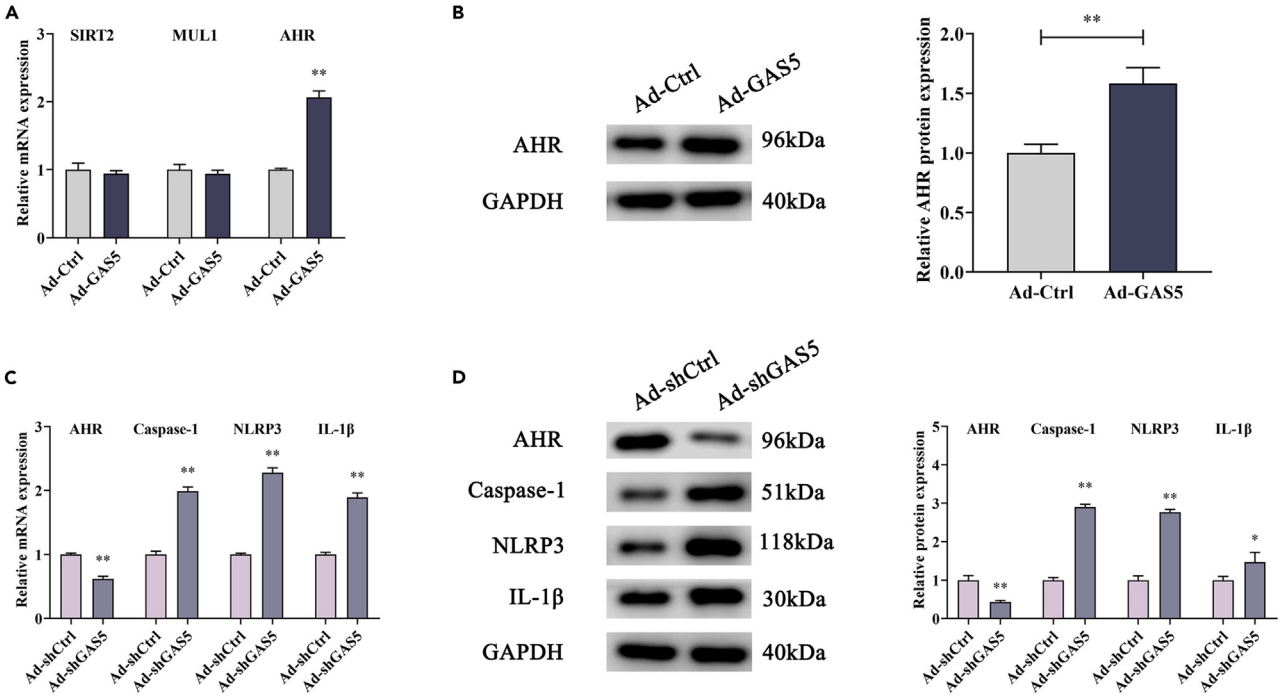

Figure 3. AHR is involved in the effects of GAS5-inhibited hepatocyte pyroptosis

Primary hepatocytes isolated from healthy controls were transduced with Ad-GAS5 or Ad-shGAS5 for 48 h.

(A) mRNA expressions of suppressors of NLRP3 (AHR, SIRT2 and MUL1).

(B) The protein level of AHR. The mRNA (C) and protein (D) expressions of AHR, Caspase-1, NLRP3, and IL-1β. Data are represented as mean ± SD and two-tailed Student's *t* test was used to assess the significance. *p < 0.05, **p < 0.01, versus Ad-Ctrl or adenovirus expressing shCtrl (Ad-shCtrl).

reporter activities (data not shown). We also generated a GAS5 mutated 3′-UTR (GAS5-Mut) luciferase reporter containing the binding sites of miR-684. There was no significant change in GAS5-Mut transfected with miR-684 mimics (Figure 4D). Also, results of the pulldown assay showed that elevated GAS5 was enriched in the biotinylated miR-684 (Bio-miR-684) group, with no change in Bio-miR-684-Mut group (Figure 4E). Direct evidence showed the co-localization of GAS5 and miR-684 in the cytoplasm of hepatocytes via fluorescence *in situ* hybridization (FISH) analysis (Figure 4F). Therefore, miR-684 targets GAS5.

miR-684 is involved in the effects of GAS5 on AHR and hepatocyte pyroptosis

We hypothesized that GAS5-mediated AHR is through regulating miR-684. Compared with the control group, elevated miR-684 was found in CCl_4-treated mice (Figure 5A), indicating a negative correlation between miR-684 and GAS5. *In* primary hepatocytes, Ad-GAS5 treatment led to a reduction in miR-684 (Figure 5B). Obviously, miR-684 mimics blocked down the reduced mRNA expressions of caspase-1, NLRP3, and IL-1β caused by GAS5 in hepatocytes (Figure 5C). Likewise, miR-684 restored the protein expressions of GAS5-inhibited caspase-1, NLRP3, and IL-1β (Figure 5D). These data suggest that miR-684 is involved in the effects of GAS5 on hepatocyte pyroptosis. AHR level was also examined in GAS5-treated hepatocytes after miR-684 mimics transfection. It was found that GAS5-induced AHR was repressed by miR-684 (Figures 5C and 5D). Taken together, GAS5-inhibited hepatocyte pyroptosis may be associated with the regulation of miR-684 and AHR.

miR-684 targets AHR

It is interesting whether AHR is a target of miR-684. Further analysis and studies were performed to investigate the relationship between miR-684 and AHR. Results of bioinformatic analysis (miRDB) showed the potential binding sites between miR-684 and AHR (Figure 6A). AHR 3′-UTR luciferase reporter containing the miR-684 sites (AHR-Wt) or miR-684 mutated sites (AHR-Mut) were generated. As shown by Figure 6B, miR-684 induced a reduction in the luciferase activity of AHR-Wt, whereas AHR-Mut not. In addition, reduced AHR was found in hepatocytes treated with miR-684 mimics (Figure 6C). Similar results were found in the AHR protein (Figure 6D). All the data suggest that AHR is a target of miR-684.

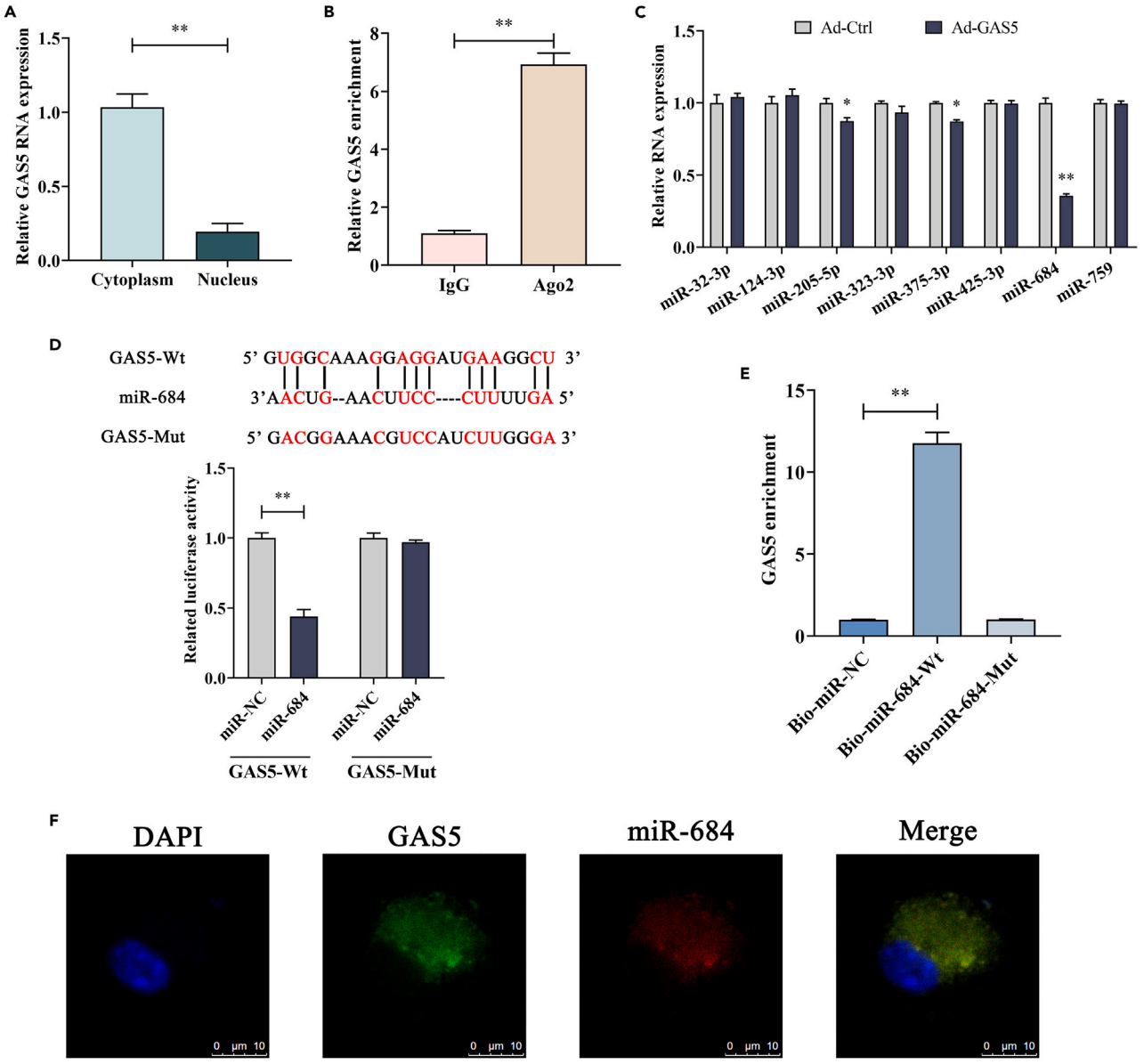

Figure 4. GAS5 is a target of miR-684

(A) The distribution of GAS5 expression in the cytoplasmic and nuclear fractions of primary hepatocytes.

(B) RIP experiments were conducted using Ago2 antibody on extracts from primary hepatocytes. The relative expression level of GAS5 was expressed as fold enrichment in Ago2 relative to IgG immunoprecipitates by qRT-PCR.

(C) Levels of miR-32-3p, miR-124-3p, miR-205-5p, miR-323-3p, miR-375-3p, miR-425-3p, miR-684, and miR-759.

(D) A schematic drawing demonstrated the putative binding sites of miR-684 concerning GAS5. Furthermore, relative luciferase activities of GAS5-Wt or GAS5-Mut were analyzed.

(E) Interaction between GAS5 and miR-684 was confirmed by pull-down assay. Bio-miR-NC is not complementary to GAS5.

(F) FISH analysis for miR-684 (red) and GAS5 (green), Scale bar: 10 μm. Data are represented as mean ± SD, two-tailed Student's *t* test was used to assess the significance between the two groups, one-way ANOVA was used to assess the significance between multiple groups. *p < 0.05, **p < 0.01.

Loss of AHR blocks down the inhibitory effects of GAS5 on hepatocyte pyroptosis

We further evaluated whether AHR is associated with the inhibitory effects of GAS5 on hepatocyte pyroptosis. Silencing of AHR led to the inhibition of AHR level in hepatocytes with GAS5 overexpression, suggesting the successful inhibition of AHR in hepatocytes (Figures 6E and 6F). Loss of AHR contributed to the suppression of GAS5-inhibited hepatocyte pyroptosis, with the increase in the mRNA levels of caspase-1, NLRP3, and IL-1β. Consistent with the mRNA results, the protein levels of caspase-1, NLRP3,

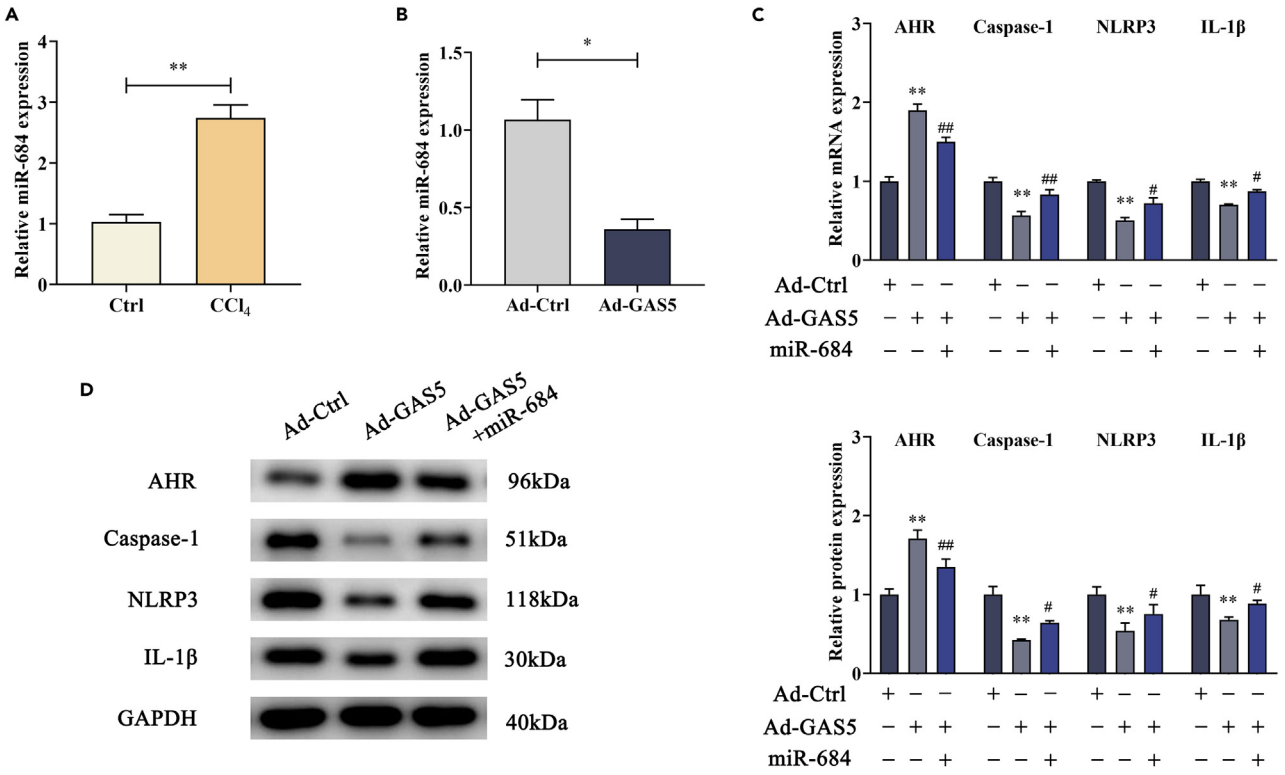

Figure 5. miR-684 is involved in the effects of GAS5 on AHR and hepatocyte pyroptosis

Primary hepatocytes were transduced with Ad-GAS5 for 48 h and then transfected with miR-684 mimic for 48 h.

(A) miR-684 level in CCl_4-treated mice.

(B) miR-684 level in GAS5-overexpressed primary hepatocytes. mRNA (C) and protein (D) expressions of AHR and pyroptosis-related markers mediated by GAS5 overexpression were restored by miR-684. Data are represented as mean ± SD, two-tailed Student's *t* test was used to assess the significance between the two groups, one-way ANOVA was used to assess the significance between multiple groups. *$p < 0.05$, **$p < 0.01$, versus Ad-Ctrl; $^{\#}p < 0.05$, $^{\#\#}p < 0.01$, versus Ad-GAS5.

and IL-1β reduced by GAS5 were restored by down-regulation of AHR (Figure 6F). In brief, our data suggest that GAS5 inhibits hepatocyte pyroptosis via regulation of miR-684 and AHR.

GAS5-inhibited hepatocyte pyroptosis contributes to the inactivation of HSCs

It is well known that HSC activation is a key event in the development of liver fibrosis. It is generally known that VX765 is a classical inhibitor of pyroptosis.[25,26] To determine whether GAS5-mediated hepatocyte pyroptosis could regulate HSC activation, HSC proliferation was examined in HSCs co-cultured with GAS5-knockdown hepatocytes (Figure 7A). Results of cell counting kit-8 (CCK8) and 5-ethyny-2'-deoxyuridine (EdU) assays showed that HSC proliferation enhanced by hepatocytes with loss of GAS5 was inhibited by VX765 treatment (Figures 7B–7D). Similarly, HSC activation markers such as Col1A1 and α-SMA were increased by hepatocytes with loss of GAS5, which was blocked down by VX765 treatment (Figures 7E and 7F). Taken together, our results suggest that GAS5-inhibited hepatocyte pyroptosis contributes to the inactivation of HSC.

DISCUSSION

Emerging studies have indicated that GAS5, abnormally expressed in a range of human diseases, is implicated in carcinogenesis, pyroptosis, inflammation, and oxidative stress.[27–29] For example, Hu et al. found that GAS5 inhibits the migration and invasion of liver cancer cells.[30] In addition, GAS5 could suppress ovarian cancer progression through the formation of inflammasome.[31] However, whether hepatocyte pyroptosis is involved in the effects of GAS5-inhibited liver fibrosis remains largely unknown. In this study, GAS5, reduced during liver fibrosis, has an inhibitory role in the progression of liver fibrosis. Next, it was found that hepatocyte pyroptosis was reduced by GAS5 treatment in CCl_4-treated mice, with a reduction in caspase-1, NLRP3, and IL-1β. Interestingly, AHR, a suppressor of NLRP3, was increased by GAS5. Loss of

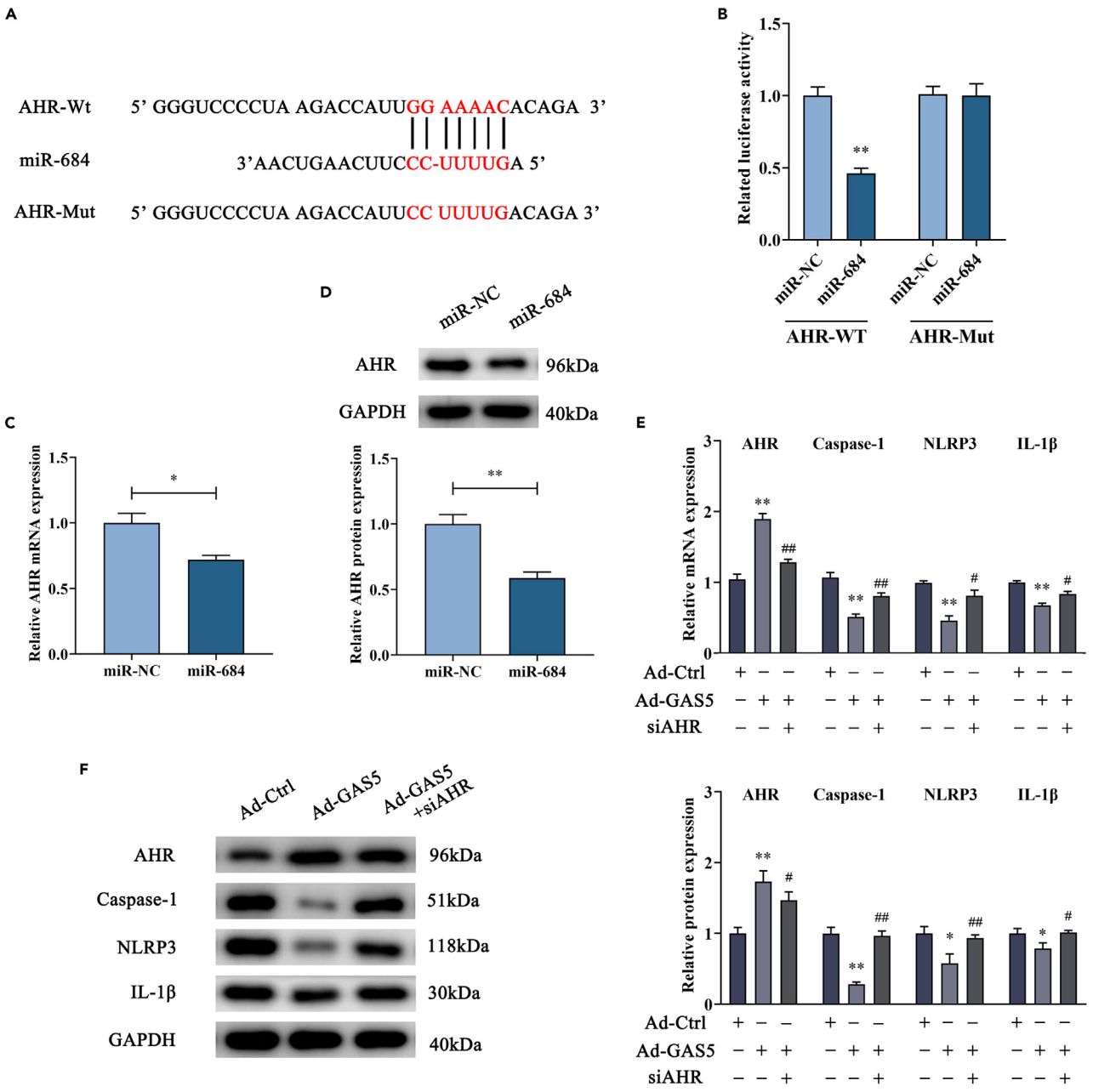

Figure 6. miR-684 targets AHR and the loss of AHR blocks down the inhibitory effects of GAS5 on hepatocyte pyroptosis

Primary hepatocytes were transduced with Ad-GAS5 for 48 h and then transfected with AHR siRNA for 48 h.

(A) A schematic drawing showed the putative binding site of miR-684 to AHR.

(B) The relative luciferase activities of AHR-Wt and AHR-Mut were also analyzed. Expressions of AHR mRNA (C) and protein (D) in primary hepatocytes treated with miR-684 mimics. Loss of AHR inhibited Ad-GAS5-mediated mRNA (E) and protein (F) expression levels of AHR and pyroptosis-related markers in hepatocytes. Data are represented as mean ± SD, two-tailed Student's *t* test was used to assess the significance between the two groups, one-way ANOVA was used to assess the significance between multiple groups. *$p < 0.05$, **$p < 0.01$, versus miR-NC or Ad-Ctrl; $^{\#}p < 0.05$, $^{\#\#}p < 0.01$, versus Ad-GAS5.

AHR or miR-684 overexpression led to the inhibition of GAS5-inhibited hepatocyte pyroptosis. Finally, both GAS5 and AHR were confirmed as targets of miR-684. Our results demonstrate that GAS5 inhibits hepatocyte pyroptosis, at least in part, via regulation of miR-684 and AHR.

It has been reported that miRNAs could act as HSC activation regulators during liver fibrosis. For example, miR-17-5p, up-regulated during liver fibrosis, promotes the development of liver fibrosis via targeting

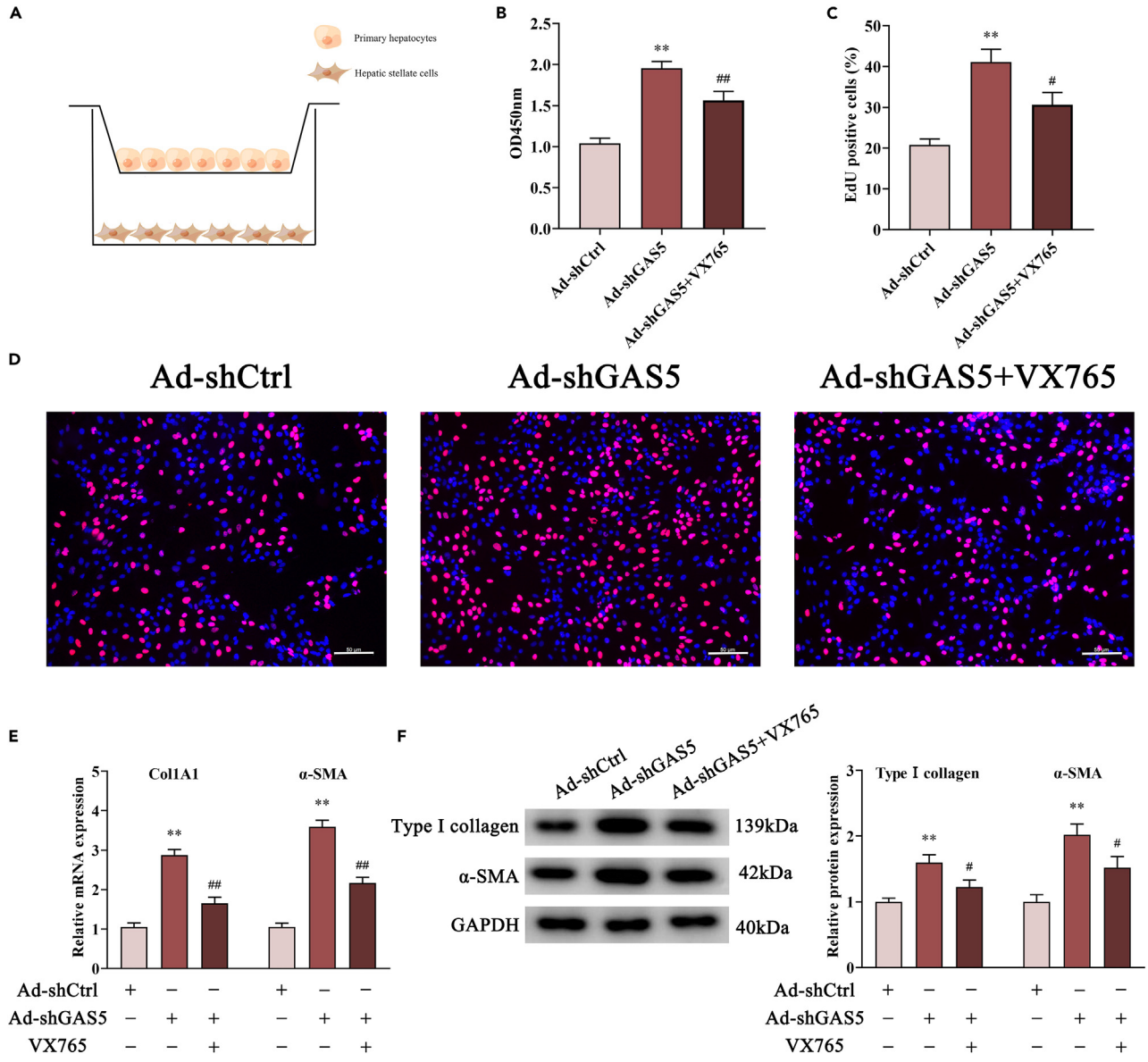

Figure 7. GAS5-inhibited hepatocyte pyroptosis contributes to the inactivation of HSCs

After treatment with pyroptosis inhibitor VX765 (50 μM) and transduction with Ad-shGAS5, primary hepatocytes were seeded in the upper compartment of the Transwell chamber, whereas in the lower chamber, mouse primary HSCs were seeded for 24 h.

(A) HSCs were co-cultured with GAS5 knockdown hepatocytes using Figdraw.

(B) CCK8 assay.

(C and D) EdU assay, Scale bar: 50 μm. The mRNA (E) and protein expressions (F) of α-SMA and Col1A1. Data are represented as mean ± SD and one-way ANOVA was used to assess the significance. **p < 0.01, versus Ad-shCtrl; #p < 0.05, ##p < 0.01, versus Ad-shGAS5.

Smad7.[32] Recently, lncRNAs have been demonstrated to act as ceRNAs to derepress miRNA targets via sponging miRNAs.[33] Previously, we demonstrated that lncRNA-SNHG7 reduces miR-378-3p level and attenuates its control on DVL2, resulting in enhanced Wnt pathway and liver fibrosis development. Herein, we found that miR-684, enhanced in CCl_4-treated mice, could be reduced by GAS5. Bioinformatic analysis revealed the potential binding sites between GAS5 and miR-684, which were confirmed by luciferase activity assays. The FISH analysis further indicated the co-localization between GAS5 and miR-684, suggesting the possible involvement of GAS5 in sponging miR-684. In addition, miR-684 overexpression blocked down the effects of GAS5 on hepatocyte pyroptosis. All the data suggest that GAS5 inhibits hepatocyte pyroptosis through sponging miR-684.

AHR, often dysregulated in various cancers, has been shown to participate in many cellular processes such as proliferation and pyroptosis.[34] It is known that AHR is a suppressor of NLRP3. For instance, AHR negatively regulates NLRP3-mediated caspase-1 activation and IL-1β secretion in macrophages by inhibiting NLRP3 transcription.[35,36] Consistent with the previous studies, our results showed that AHR could be increased by GAS5. Interestingly, AHR is a target of miR-684. Loss of AHR led to the inhibition of GAS5-inhibited hepatocyte pyroptosis. Combined with these, GAS5 inhibits hepatocyte pyroptosis, at least in part, via regulation of miR-684 and its target AHR.

Pyroptosis of hepatocytes, the main cells in the liver, has been shown to play a crucial role in the regulation of HSC activation and liver fibrosis development. Wree et al. found that NLRP3 inflammasome activation results in hepatocyte pyroptosis, liver inflammation, and fibrosis.[5] NLRP3 inflammasome induces pyroptosis by caspase-1, releasing inflammatory mediators such as IL-1β, and finally effectively activates HSCs.[5,37] Likewise, Gaul et al. demonstrated that inflammatory mediators released by pyroptotic hepatocytes contribute to the activation of HSCs.[2] In this study, we examined the effects of hepatocyte pyroptosis on HSC activation. It was found that Ad-shGAS5-induced hepatocyte pyroptosis resulted in the enhancement in HSC activation, which was inhibited by VX765 treatment. The reason for the change in HSC activation caused by GAS5-mediated hepatocyte pyroptosis may be associated with inflammatory mediators such as IL-1β. Collectively, our results suggest that GAS5 overexpression prevents liver fibrosis by inhibiting NLRP3-mediated pyroptosis, leading to the reduction in the release of inflammatory mediators and the suppression of HSC activation.

In conclusion, GAS5 inhibits hepatocyte pyroptosis via the regulation of miR-684 and AHR, contributing to the suppression of HSC activation and liver fibrosis. Our findings provide an insight into cellular interactions between hepatocytes and HSCs.

Limitations of the study

In this study, we used a liver fibrosis model in CCl_4-treated mice. The findings suggest that GAS5 inhibits pyroptosis in hepatocytes by regulating miR-684 and AHR, which contributes to the inhibition of HSC activation and liver fibrosis. However, further work is needed. For example, organoids could be used to confirm the mechanism of GAS5-inhibited liver fibrosis. In addition, clinical samples can also be collected to explore the feasibility of using GAS5 as a biomarker in patients with liver fibrosis.

STAR★METHODS

Detailed methods are provided in the online version of this paper and include the following:

- KEY RESOURCES TABLE
- RESOURCE AVAILABILITY
  - Lead contact
  - Materials availability
  - Data and code availability
- EXPERIMENTAL MODEL AND STUDY PARTICIPANT DETAILS
  - CCl_4 liver injury model
  - Isolation of mouse primary hepatocytes
  - Isolation and extraction of primary HSCs
- METHOD DETAILS
  - Adenoviral transduction
  - qRT-PCR
  - Western Blot analysis
  - Liver histological staining
  - Immunohistochemistry
  - Immunofluorescence staining
  - Measurement of serum ALT and AST
  - Cell co-culture
  - EdU assays
  - FISH
  - RIP assay
  - Pull-down assay with the Bio-miR-684

- CCK8 assay
- Luciferase reporter assay

- QUANTIFICATION AND STATISTICAL ANALYSIS

SUPPLEMENTAL INFORMATION

Supplemental information can be found online at https://doi.org/10.1016/j.isci.2023.107326.

ACKNOWLEDGMENTS

The project was supported by the National Natural Science Foundation of China (No. 81873576), Wenzhou Municipal Science and Technology Bureau (No. Y20220023), Key Laboratory of Clinical Laboratory Diagnosis and Translational Research of Zhejiang Province (No. 2022E10022) and the project of Wenzhou Medical University Basic Scientific Research (No. KYYW201904).

AUTHOR CONTRIBUTIONS

Conceptualization, Z.Y. and J.Z.; methodology, X.L., Y.J., and X.L.; software, Y.H.; validation, Y.T.; formal analysis, Z.L., X.L., and R.Z.; investigation, R.Z.; resources, Y.J., X.L., and R.Z.; data curation, J.Z. and Z.L.; writing—original draft preparation, Z.L. and R.Z.; writing—review and editing, Z.L. and J.Z.; visualization, R.Z. and J.Z.; supervision, Z.Y.; project administration, Z.Y. and J.Z.; funding acquisition, L.Z., Z.Y., and J.Z. All authors have read and agreed to the published version of the manuscript.

DECLARATION OF INTERESTS

The authors declare no competing interests.

INCLUSION AND DIVERSITY

We support inclusive, diverse, and equitable conduct of research.

Received: April 1, 2023
Revised: May 31, 2023
Accepted: July 5, 2023
Published: July 13, 2023

REFERENCES

1. Ye, D., Heraud, P., Parnpai, R., and Li, T. (2017). Reversal of experimental liver damage after transplantation of stem-derived cells detected by FTIR spectroscopy. Stem Cell. Int. *2017*, 4585169. https://doi.org/10.1155/2017/4585169.

2. Gaul, S., Leszczynska, A., Alegre, F., Kaufmann, B., Johnson, C.D., Adams, L.A., Wree, A., Damm, G., Seehofer, D., Calvente, C.J., et al. (2021). Hepatocyte pyroptosis and release of inflammasome particles induce stellate cell activation and liver fibrosis. J. Hepatol. *74*, 156–167. https://doi.org/10.1016/j.jhep.2020.07.041.

3. Shojaie, L., Iorga, A., and Dara, L. (2020). Cell death in liver diseases: a review. Int. J. Mol. Sci. *21*, 9682. https://doi.org/10.3390/ijms21249682.

4. Geng, Y., Ma, Q., Liu, Y.N., Peng, N., Yuan, F.F., Li, X.G., Li, M., Wu, Y.S., Li, B.l., Song, W.b., et al. (2015). Heatstroke induces liver injury via IL-1β and HMGB1-induced pyroptosis. J. Hepatol. *63*, 622–633. https://doi.org/10.1016/j.jhep.2015.04.010.

5. Wree, A., Eguchi, A., McGeough, M.D., Pena, C.A., Johnson, C.D., Canbay, A., Hoffman, H.M., and Feldstein, A.E. (2014). NLRP3 inflammasome activation results in hepatocyte pyroptosis, liver inflammation, and fibrosis in mice. Hepatology *59*, 898–910. https://doi.org/10.1002/hep.26592.

6. Yang, Y., Liu, P.Y., Bao, W., Chen, S.J., Wu, F.S., and Zhu, P.Y. (2020). Hydrogen inhibits endometrial cancer growth via a ROS/NLRP3/caspase-1/GSDMD-mediated pyroptotic pathway. BMC Cancer *20*, 28. https://doi.org/10.1186/s12885-019-6491-6.

7. Meng, Q.Q., Feng, Z.C., Zhang, X.L., Hu, L.Q., Wang, M., Zhang, H.F., and Li, S.M. (2019). PPAR-gamma activation exerts an anti-inflammatory effect by suppressing the NLRP3 inflammasome in spinal cord-derived neurons. Mediat. Inflamm. *2019*, 6386729. https://doi.org/10.1155/2019/6386729.

8. Dufies, O., Doye, A., Courjon, J., Torre, C., Michel, G., Loubatier, C., Jacquel, A., Chaintreuil, P., Majoor, A., Guinamard, R.R., et al. (2021). Escherichia coli Rho GTPase-activating toxin CNF1 mediates NLRP3 inflammasome activation via p21-activated kinases-1/2 during bacteraemia in mice. Nat. Microbiol. *6*, 401–412. https://doi.org/10.1038/s41564-020-00832-5.

9. Wang, M., Jiang, S., Zhang, Y., Li, P., and Wang, K. (2019). The multifaceted roles of pyroptotic cell death pathways in cancer. Cancers *11*, 1313. https://doi.org/10.3390/cancers11091313.

10. Amir, M., and Czaja, M.J. (2018). Inflammasome-mediated inflammation and fibrosis: It is more than just the IL-1beta. Hepatology *67*, 479–481. https://doi.org/10.1002/hep.29491.

11. Chen, L., Zhou, Q., Liu, E., Zhang, J., Duan, L., Zhu, D., Chen, J., and Duan, Y. (2019). rSjp40 inhibits activated hepatic stellate cells by promoting nuclear translocation of YB1 and inducing BMP-7/Smad1/5/8 pathway. Parasit. Vectors *12*, 279. https://doi.org/10.1186/s13071-019-3539-z.

12. Mourtada-Maarabouni, M., Pickard, M.R., Hedge, V.L., Farzaneh, F., and Williams, G.T. (2009). GAS5, a non-protein-coding RNA, controls apoptosis and is downregulated in breast cancer. Oncogene *28*, 195–208. https://doi.org/10.1038/onc.2008.373.

13. Yacqub-Usman, K., Pickard, M.R., and Williams, G.T. (2015). Reciprocal regulation of GAS5 lncRNA levels and mTOR inhibitor action in prostate cancer cells. Prostate *75*,

693–705. https://doi.org/10.1002/pros.22952.

14. Long, X., Song, K., Hu, H., Tian, Q., Wang, W., Dong, Q., Yin, X., and Di, W. (2019). Long non-coding RNA GAS5 inhibits DDP-resistance and tumor progression of epithelial ovarian cancer via GAS5-E2F4-PARP1-MAPK axis. J. Exp. Clin. Cancer Res. *38*, 345. https://doi.org/10.1186/s13046-019-1329-2.

15. Li, K., and Chen, Y. (2020). CYP2C8 regulated by GAS5/miR-382-3p exerts anti-cancerous properties in liver cancer. Cancer Biol. Ther. *21*, 1145–1153. https://doi.org/10.1080/15384047.2020.1840886.

16. Han, M.H., Lee, J.H., Kim, G., Lee, E., Lee, Y.R., Jang, S.Y., Lee, H.W., Chun, J.M., Han, Y.S., Yoon, J.S., et al. (2020). Expression of the long noncoding RNA GAS5 correlates with liver fibrosis in patients with nonalcoholic fatty liver disease. Genes *11*, 545. https://doi.org/10.3390/genes11050545.

17. Yu, F., Zheng, J., Mao, Y., Dong, P., Lu, Z., Li, G., Guo, C., Liu, Z., and Fan, X. (2015). Long non-coding RNA growth arrest-specific transcript 5 (GAS5) inhibits liver fibrogenesis through a mechanism of competing endogenous RNA. J. Biol. Chem. *290*, 28286–28298. https://doi.org/10.1074/jbc.M115.683813.

18. Mo, R., Li, J., Chen, Y., and Ding, Y. (2022). lncRNA GAS5 promotes pyroptosis in COPD by functioning as a ceRNA to regulate the miR2233p/NLRP3 axis. Mol. Med. Rep. *26*, 219. https://doi.org/10.3892/mmr.2022.12735.

19. Qiao, H., Zhou, Y., Qin, X., Cheng, J., He, Y., and Jiang, Y. (2018). NADPH oxidase signaling pathway mediates mesenchymal stem cell-induced inhibition of hepatic stellate cell activation. Stem Cells Int. *2018*, 1239143. https://doi.org/10.1155/2018/1239143.

20. Dwivedi, D.K., Jena, G., and Kumar, V. (2020). Dimethyl fumarate protects thioacetamide-induced liver damage in rats: Studies on Nrf2, NLRP3, and NF-kappaB. J. Biochem. Mol. Toxicol. *34*, e22476. https://doi.org/10.1002/jbt.22476.

21. Li, J., Kong, L., Huang, H., Luan, S., Jin, R., and Wu, F. (2020). ASIC1a inhibits cell pyroptosis induced by acid-induced activation of rat hepatic stellate cells. FEBS Open Bio *10*, 1044–1055. https://doi.org/10.1002/2211-5463.12850.

22. Chen, Z., He, M., Chen, J., Li, C., and Zhang, Q. (2020). Long non-coding RNA SNHG7 inhibits NLRP3-dependent pyroptosis by targeting the miR-34a/SIRT1 axis in liver cancer. Oncol. Lett. *20*, 893–901. https://doi.org/10.3892/ol.2020.11635.

23. Kim, H.Y., Choi, Y.J., Kim, S.K., Kim, H., Jun, D.W., Yoon, K., Kim, N., Hwang, J., Kim, Y.M., Lim, S.C., and Kang, K.W. (2021). Auranofin prevents liver fibrosis by system Xc-mediated inhibition of NLRP3 inflammasome. Commun. Biol. *4*, 824. https://doi.org/10.1038/s42003-021-02345-1.

24. Xie, F., Li, L., Luo, Y., Chen, R., and Mei, J. (2021). Long non-coding RNA LINC00488 facilitates thyroid cancer cell progression through miR-376a-3p/PON2. Biosci. Rep. *41*. BSR20201603. https://doi.org/10.1042/BSR20201603.

25. Wang, G., Wei, W., Jiang, Z., Jiang, J., Han, J., Zhang, H., Hu, J., Zhang, P., Li, X., Chen, T., et al. (2022). Talaromyces marneffei activates the AIM2-caspase-1/-4-GSDMD axis to induce pyroptosis in hepatocytes. Virulence *13*, 963–979. https://doi.org/10.1080/21505594.2022.2080904.

26. Teng, J.F., Mei, Q.B., Zhou, X.G., Tang, Y., Xiong, R., Qiu, W.Q., Pan, R., Law, B.Y.K., Wong, V.K.W., Yu, C.L., et al. (2020). Polyphyllin VI induces caspase-1-mediated pyroptosis via the induction of ROS/NF-kappaB/NLRP3/GSDMD signal axis in non-small cell lung cancer. Cancers *12*, 193. https://doi.org/10.3390/cancers12010193.

27. Xie, C., Wu, W., Tang, A., Luo, N., and Tan, Y. (2019). lncRNA GAS5/miR-452-5p reduces oxidative stress and pyroptosis of high-glucose-stimulated renal tubular cells. Diabetes Metab. Syndr. Obes. *12*, 2609–2617. https://doi.org/10.2147/DMSO.S228654.

28. Ni, W., Yao, S., Zhou, Y., Liu, Y., Huang, P., Zhou, A., Liu, J., Che, L., and Li, J. (2019). Long noncoding RNA GAS5 inhibits progression of colorectal cancer by interacting with and triggering YAP phosphorylation and degradation and is negatively regulated by the m(6)A reader YTHDF3. Mol. Cancer *18*, 143. https://doi.org/10.1186/s12943-019-1079-y.

29. Peng, T., Ji, D., and Jiang, Y. (2021). Long non-coding RNA GAS5 suppresses rheumatoid arthritis progression via miR-128-3p/HDAC4 axis. Mol. Cell. Biochem. *476*, 2491–2501. https://doi.org/10.1007/s11010-021-04098-1.

30. Hu, L., Ye, H., Huang, G., Luo, F., Liu, Y., Liu, Y., Yang, X., Shen, J., Liu, Q., and Zhang, J. (2016). Long noncoding RNA GAS5 suppresses the migration and invasion of hepatocellular carcinoma cells via miR-21. Tumour Biol. *37*, 2691–2702. https://doi.org/10.1007/s13277-015-4111-x.

31. Li, J., Yang, C., Li, Y., Chen, A., Li, L., and You, Z. (2018). LncRNA GAS5 suppresses ovarian cancer by inducing inflammasome formation. Biosci. Rep. *38*. BSR20171150. https://doi.org/10.1042/BSR20171150.

32. Zhou, G., Li, C., Zhan, Y., Zhang, R., Lv, B., Geng, W., and Zheng, J. (2020). Pinostilbene hydrate suppresses hepatic stellate cell activation via inhibition of miR-17-5p-mediated Wnt/beta-catenin pathway. Phytomedicine *79*, 153321. https://doi.org/10.1016/j.phymed.2020.153321.

33. Yu, F., Dong, P., Mao, Y., Zhao, B., Huang, Z., and Zheng, J. (2019). Loss of lncRNA-SNHG7 promotes the suppression of hepatic stellate cell activation via miR-378a-3p and DVL2. Mol. Ther. Nucleic Acids *17*, 235–244. https://doi.org/10.1016/j.omtn.2019.05.026.

34. Deuster, E., Mayr, D., Hester, A., Kolben, T., Zeder-Göß, C., Burges, A., Mahner, S., Jeschke, U., Trillsch, F., and Czogalla, B. (2019). Correlation of the aryl hydrocarbon receptor with FSHR in ovarian cancer patients. Int. J. Mol. Sci. *20*, 2862. https://doi.org/10.3390/ijms20122862.

35. Luborsky, J., Barua, A., Edassery, S., Bahr, J.M., and Edassery, S.L. (2020). Inflammasome expression is higher in ovarian tumors than in normal ovary. PLoS One *15*, e0227081. https://doi.org/10.1371/journal.pone.0227081.

36. Ngui, I., Perera, A., and Eri, R.J.M. (2020). Does NLRP3 inflammasome and aryl hydrocarbon receptor play an interlinked role in bowel inflammation and colitis-associated colorectal cancer? Molecules *25*, 2427. https://doi.org/10.3390/molecules25102427.

37. Sharma, B.R., and Kanneganti, T.D. (2021). NLRP3 inflammasome in cancer and metabolic diseases. Nat. Immunol. *22*, 550–559. https://doi.org/10.1038/s41590-021-00886-5.

38. Wang, Q., Wei, S., Zhou, H., Li, L., Zhou, S., Shi, C., Shi, Y., Qiu, J., and Lu, L. (2020). MicroRNA-98 inhibits hepatic stellate cell activation and attenuates liver fibrosis by regulating hlf expression. Front. Cell Dev. Biol. *8*, 513. https://doi.org/10.3389/fcell.2020.00513.

39. Li, W.C., Ralphs, K.L., and Tosh, D. (2010). Isolation and culture of adult mouse hepatocytes. Methods Mol. Biol. *633*, 185–196. https://doi.org/10.1007/978-1-59745-019-5_13.

40. Maschmeyer, P., Flach, M., and Winau, F. (2011). Seven steps to stellate cells. J. Vis. Exp. https://doi.org/10.3791/2710.

41. Zhou, G., Li, C., Zhang, R., Zhan, Y., Lin, L., Lang, Z., Tao, Q., and Zheng, J. (2022). Kaempferol inhibits hepatic stellate cell activation by regulating miR-26b-5p/Jag1 axis and notch pathway. Front. Pharmacol. *13*, 881855. https://doi.org/10.3389/fphar.2022.881855.

42. Yu, F., Geng, W., Dong, P., Huang, Z., and Zheng, J. (2018). LncRNA-MEG3 inhibits activation of hepatic stellate cells through SMO protein and miR-212. Cell Death Dis. *9*, 1014. https://doi.org/10.1038/s41419-018-1068-x.

43. Yu, F., Chen, B., Dong, P., and Zheng, J. (2020). HOTAIR epigenetically modulates PTEN expression via MicroRNA-29b: a novel mechanism in regulation of liver fibrosis. Mol. Ther. *28*, 2703. https://doi.org/10.1016/j.ymthe.2020.10.021.

STAR★METHODS

KEY RESOURCES TABLE

REAGENT or RESOURCE	SOURCE	IDENTIFIER
Antibodies		
Rabbit antibody-type I collagen	ABCAM	Cat#ab270993
Rabbit antibody-α-SMA	ABCAM	Cat#ab5694 RRID: AB_2223021
Rabbit antibody-AHR	ABCAM	Cat#ab308215
Rabbit antibody-Caspase-1	ABCAM	Cat#ab138483 RRID: AB_2888675
Mouse antibody-Caspase-3	ABCAM	Cat#ab13585 RRID: AB_300480
Rabbit antibody-NLRP3	ABCAM	Cat#ab263899 RRID: AB_2889890
Rabbit antibody-IL-1β	ABCAM	Cat#ab254360
Rabbit antibody-GAPDH	ABCAM	Cat#ab9485 RRID: AB_307275
Goat anti-rabbit IgG (H+L), HRP conjugate antibody	proteintech	Cat#SA00001-2 RRID: AB_2722564
Donkey anti-Rabbit IgG (H+L) Highly Cross-Adsorbed Secondary Antibody, Alexa Fluor 594	Thermo Fisher	Cat# A-21207 RRID: AB_141637
Chemicals, peptides, and recombinant proteins		
VX765	Med Chem Express	Cat#273404-37-8
Experimental models: Cell lines		
primary hepatocytes	C57BL/6J mice	N/A
primary HSCs	C57BL/6J mice	N/A
Experimental models: Organisms/strains		
C57BL/6J mice (8 weeks, 18-22g)	Zhejiang Weitong Lihua Experimental Animal Technology Co. Ltd	SYXK-(zhe)-2021-0020
Oligonucleotides		
RNA purification kit	Norgen	Cat#17200
miRNeasy mini kit	QIAGEN	Cat#217004
ReverTra Ace qPCR RT Kit	TOYOBO	Cat#FSQ-101
SYBR Green Real time PCR Master Mix	TOYOBO	Cat#QPK-201
See Table S1 for the primers sequences	This paper	N/A
Recombinant DNA		
GAS5: 5′-CCATCACAGAGGTCCACACTGCCATTCCTGCT-3′	Wuhan Sevier Biotechnology Co., Ltd	N/A
mir-684:5′-TTGACTTGAAGGGAAAACT-3′	Wuhan Sevier Biotechnology Co., Ltd	N/A
Software and algorithms		
ImageJ	National Institutes of Health (NIH)	https://imagej.nih.gov/ij/
SPSS 22.0	Chicago	https://www.ibm.com/support/pages/spss-statistics-220-available-download
Other		
Sirius Red Staining Kit	Polysciences	Cat#24901

(*Continued on next page*)

Continued

REAGENT or RESOURCE	SOURCE	IDENTIFIER
Masson Staining Kit	ABCAM	Cat#ab150669
HE Staining Kit	Solarbio	Cat#G1120
ALT Kit	Nanjing Jiancheng Bioengineering Institute	Cat#C009-2-1
AST Kit	Nanjing Jiancheng Bioengineering Institute	Cat#C010-2-1
EdU assay kit	RiboBio	Cat#C10310-3
EZ-Magna RIP kit	Millipore Corporation	Cat#17-700
CCK8 Kit	Dojindo	Cat#CK04

RESOURCE AVAILABILITY

Lead contact

Further information and requests for resources, reagents and original data should be directed to and will be fulfilled by the lead contact, Jianjian Zheng (zjj@wmu.edu.cn).

Materials availability

This work did not generate new unique reagents.

Data and code availability

- All data reported in this paper will be shared by the lead contact upon request.
- This paper does not report original code.
- Any additional information required to reanalyze the data reported in this paper is available from the lead contact upon request.

EXPERIMENTAL MODEL AND STUDY PARTICIPANT DETAILS

CCl_4 liver injury model

The experiment with animals was conducted as previously described.[38] Eight-week-old male C57BL/6J were provided by Zhejiang Weitong Lihua Experimental Animal Technology Co. Ltd. Mice (n=6) were injected twice weekly with CCl_4 (10%, 7 ml/kg) in olive oil for 8 weeks to induce liver fibrosis. The control group consisted of mice (n=6) treated with olive oil.

Mouse liver fibrosis was induced by injecting intraperitoneally CCl_4 (10%, 7 ml/kg) twice a week for 6 weeks or a vehicle (olive oil). Ad-Ctrl or Ad-GAS5 (1×10^9 pfu/100 mL) were injected into mice via the tail vein every two weeks for six weeks while they were receiving CCl_4 treatment. All mice were divided into four groups at random: olive oil (n=6), CCl_4 (n=6), CCl_4+Ad-Ctrl (n=6) and CCl_4+Ad-GAS5 (n=6). All animal handling procedures were performed in compliance with the People's Republic of China legislation for the care and use of laboratory animals. All animal studies were approved by the Laboratory Animal Ethics Committee of the Wenzhou Medical University. The registration number was wydw2022-0688. In the end, mice were anesthetized by intraperitoneal injection of 1% sodium pentobarbital (50 mg/kg), and their livers were taken to be analyzed.

Isolation of mouse primary hepatocytes

The primary hepatocyte isolation was from livers of male C57BL/6J mouse using a two-step perfusion method.[39] The following day, the hepatocytes were seeded on collagen-coated culture dishes for the experiment.

Isolation and extraction of primary HSCs

As previously described,[40] the male C57BL/6J mouse livers were carefully excised and divided into small pieces. Incubating the liver pieces in PBS containing Trypsin 0.05% and EDTA 0.053 mmol/L at 37°C. After digestion, the tissue was mechanically separated softly until there was no obvious tissue mass. 70-mm cell

strainer was used to strain the cells, and DMEM supplemented with 10% FBS was used twice to wash them. HSCs were cultured in humidified air containing 5% CO_2 at 37°C.

METHOD DETAILS

Adenoviral transduction

Ad-shGAS5 or Ad-GAS5 were constructed. Primary hepatocytes were transduced for 48 h with Ad-shGAS5 or Ad-GAS5 and then collected for further research.

qRT-PCR

The miRNeasy mini kit (QIAGEN, Valencia, CA, USA) was used to obtain total RNA from cells and liver tissues. To reverse-transcribe total RNA into cDNA, ReverTra Ace qPCR RT Kit (Toyobo, Osaka, Japan) was used. The cytoplasmic or nuclear components of GAS5 were extracted from primary hepatocytes using RNA purification kits (Norgen, Thorold, Canada). Gene expression was detected using qRT-PCR with SYBR Green Real time PCR Master Mix (Toyobo, Osaka, Japan). The relative abundance of miRNAs was normalized using U6 small nuclear RNA (Applied Biosystems, Foster City, CA, USA). The cycle threshold (Ct) is defined as the number of cycles required for the fluorescent signal to cross the threshold. The relative expressions of GAS5, mRNAs, and miRNAs were calculated using $2^{-\Delta\Delta Ct}$ method, with $\Delta Ct = Ct_{target} - Ct_{reference}$, $-\Delta\Delta Ct = -(\text{sample } \Delta Ct - \text{control } \Delta Ct)$. The primers were shown in Table S1.

Western Blot analysis

The tissues and cells were lysed with ice-cold lysis buffer (50 mM Tris-HCl [pH 7.4], 100 mM 2-mercaptoethanol, 2% [w/v] SDS, 10% glycerol). SDS-PAGE was used to separate total proteins. After SDS-PAGE, proteins were transferred to PVDF membranes (Millipore, Billerica, MA). After blocking, at 4°C, the incubation of membranes was carried out using primary antibodies against type I collagen, α-SMA, AHR, Caspase-1, Caspase-3, NLRP3, IL-1β and GAPDH (Abcam, Cambridge, UK) overnight. And then the secondary goat anti-rabbit IgG (Proteintech, China) was used at 37°C for 1 h. GAPDH was used as an internal control.

Liver histological staining

Liver tissues were fixed and then paraffin-embedded, which were used for Sirius Red staining, Masson staining and HE staining. Sirius Red staining was performed using the Sirius Red Staining Kit (Polysciences, Germany). Masson staining was performed following the manufacture's protocols (Abcam, Cambridge, UK). HE staining was performed by HE Staining Kit (Solarbio, Beijing, China). Leica DM4B microscope was used to capture images.

Immunohistochemistry

Literature-based immunohistochemistry was performed.[41] The rehydrated tissue slides were heated in an antigen retrieval solution containing 10 mM EDTA (pH 8.0). Then, the sections were blocked with 10% BSA for 1 h at 37°C and incubated with anti-α-SMA primary antibody for at least 12 h at 4°C. Afterward, the sections were incubated with a secondary antibody conjugated with horseradish peroxidase for 1 h. Finally, α-SMA positive areas were quantified under the microscope (Carl Zeiss, Germany). The α-SMA expression was detected by brown staining.

Immunofluorescence staining

For liver specimens, liver sections were permeabilized with 0.5 % Triton X-100 for 20 min and blocked in 5 % BSA solution for 40 min in room temperature, followed by incubating with primary anti-Caspase-1 (Affinity Biosciences, Zhenjiang, China), anti-NLRP3 (Abcam, Cambridge, UK) and anti-IL-1β (Abcam, Cambridge, UK) antibodies overnight at 4°C. Then, liver sections were stained with fluorescent secondary antibodies conjugated with Alexa Fluor 594 (ThermoFisher, Madrid, Spain). For nuclear counterstaining, 4,6-diamidino-2-phenylindole (DAPI, KeyGEN, Nanjing, China) was applied, and cells were observed using a fluorescence microscope (Nikon).

Measurement of serum ALT and AST

Serum samples were separated from whole blood by centrifugation. Then, serum ALT and AST were measured using ALT Kit and AST Kit (Nanjing Jiancheng Bioengineering Institute, Nanjing, China).

Cell co-culture

After treatment with or without pyroptosis inhibitor VX765 (50 μM),[25] hepatocytes transduced with Ad-shGAS5 were used for subsequent studies. Cells with Ad-shCtrl treatment was used as the control group. In the upper compartment of the Transwell chamber (0.4 μm pore size, 24 mm diameter, Corning Costar, MA, USA), mouse primary hepatocytes were seeded, whereas in the lower chamber, mouse primary HSCs were seeded for 24 h.

EdU assays

The EdU assay was performed using EdU assay kit (RiboBio, Guangzhou, China). Briefly, cells were treated with EdU. Cell nuclei were stained with DAPI (KeyGEN, Nanjing, China). and visualized under a microscope.

FISH

With minor adjustments, the double FISH assay was carried out in cells as previously presented.[42] Biotin-labeled probes specific to GAS5 as well as Dig-labeled miR-684 probes (Wuhan Sevier Biotechnology Co., Ltd, Wuhan, China) were employed in the hybridization. DAPI was used as a counterstained for nuclei. Images were obtained from a Leica TCS SP2 AOBS confocal microscope (Leica Microsystems, Mannheim, Germany).

RIP assay

According to manufacturer's instructions, the RIP assay was performed using the EZ-Magna RIP kit (Millipore Corporation, USA). Briefly, total RNA from primary hepatocytes was extracted using RIP lysis buffer, and then the incubation with RIP buffer including magnetic beads and an anti-Ago2 antibody (Abcam, Cambridge, UK). Isotype-matched IgG was used for negative control. After the incubation of samples with Proteinase K, immunoprecipitated RNA was isolated. Following TRIzol and ethanol precipitation, the enrichment was measured by qRT-PCR.

Pull-down assay with the Bio-miR-684

Biotin pull-down was conducted as previously mentioned.[17,33] Briefly, after 48 h of primary hepatocytes transfected with Bio-miR-684-Wt, Bio-miR-684-Mut, or Bio-miR-NC, the cells were washed with PBS, briefly vortexed, and incubated in lysis buffer for 10 min. After removing RNA and protein complexes, the incubation of lysates was done with streptavidin-coated magnetic beads (Life Technologies, Germany) at 4°C for 4 h. Then three times with low-salt buffer, and once with high-salt buffer were also performed. With the use of TRIzol reagent (Life Technologies, Germany), the isolation of bound RNAs was carried out. The GAS5 expression level was detected by qRT-PCR.

CCK8 assay

CCK8 assays were performed with a CCK8 Kit (Dojindo, Shanghai, China). HSCs were plated in 96-well plates at a density of 5×10^4 cells/ml. Prior to measuring, 10 μl of CCK-8 solution was added to each well and the plate was incubated for 3 h at 37°C, and their absorbance at 450 nm was measured.

Luciferase reporter assay

Lipofectamine-mediated gene transfer was used to cotransfect pmirGLO-GAS5 and pmirGLO-AHR with predicted miRNAs or miR-NC into HEK293T cells as described previously.[43] After 48 h of transfection, relative luciferase activity was normalized to Renilla luciferase activity (Invitrogen, USA).

QUANTIFICATION AND STATISTICAL ANALYSIS

The data were obtained from at least three independent experiments and shown as the mean ± standard deviation. Differences between multiple groups were estimated by using one-way ANOVA. A two-tailed Student's t-test was used to compare the differences between the two groups. The quantification of Masson staining, Sirius Red staining and immunohistochemistry were performed by ImageJ software. $P < 0.05$ was considered statistically significant. All data were analyzed using SPSS 22.0 statistical software (Chicago, IL, USA).